

Species-agnostic polymeric formulations for inhalable messenger RNA delivery to the lung

Received: 16 September 2021

Accepted: 11 October 2022

Published online: 28 November 2022

 Check for updates

Laura Rotolo^{1,12}, Daryll Vanover^{1,12}, Nicholas C. Bruno^{2,12}, Hannah E. Peck¹, Chiara Zurla¹, Jackelyn Murray³, Richard K. Noel⁴, Laura O'Farrell⁴, Mariluz Araínga⁵, Nichole Orr-Burks³, Jae Yeon Joo¹, Lorena C. S. Chaves¹, Younghun Jung¹, Jared Beyersdorf¹, Sanjeev Gumber⁶, Ricardo Guerrero-Ferreira⁷, Santiago Cornejo⁸, Merrilee Thoresen⁸, Alicia K. Olivier⁸, Katie M. Kuo², James C. Gumbart^{2,9}, Amelia R. Woolums⁸, Francois Villinger⁵, Eric R. Lafontaine³, Robert J. Hogan^{3,10}, M. G. Finn^{2,11} & Philip J. Santangelo¹✉

Messenger RNA has now been used to vaccinate millions of people. However, the diversity of pulmonary pathologies, including infections, genetic disorders, asthma and others, reveals the lung as an important organ to directly target for future RNA therapeutics and preventatives. Here we report the screening of 166 polymeric nanoparticle formulations for functional delivery to the lungs, obtained from a combinatorial synthesis approach combined with a low-dead-volume nose-only inhalation system for mice. We identify P76, a poly- β -amino-thio-ester polymer, that exhibits increased expression over formulations lacking the thiol component, delivery to different animal species with varying RNA cargos and low toxicity. P76 allows for dose sparing when delivering an mRNA-expressed Cas13a-mediated treatment in a SARS-CoV-2 challenge model, resulting in similar efficacy to a 20-fold higher dose of a neutralizing antibody. Overall, the combinatorial synthesis approach allowed for the discovery of promising polymeric formulations for future RNA pharmaceutical development for the lungs.

The flexibility of nucleic-acid-based drugs allows a variety of therapeutic proteins to be encoded for use as a treatment, prophylactic or vaccine. Efficacious delivery of cargo to a target organ enables the development of multiple therapeutic programs with minimal vehicle redesign requirements. Given the large number of pulmonary pathogens and diseases including SARS-CoV-2, influenza and cystic fibrosis

(CF), among others, the efficient delivery of messenger RNA (mRNA) to the lungs represents a promising approach for both treatment and prevention.

To date, the administration of mRNA to the lungs has largely consisted of the academic demonstrations of polyethylenimine and lipid nanoparticle deliveries to mice, with few formulations reaching

¹Wallace H. Coulter Department of Biomedical Engineering, Georgia Institute of Technology and Emory University, Atlanta, GA, USA. ²School of Chemistry and Biochemistry, Georgia Institute of Technology, Atlanta, GA, USA. ³Department of Infectious Diseases, College of Veterinary Medicine University of Georgia, Athens, GA, USA. ⁴Physiological Research Laboratory, Georgia Institute of Technology, Atlanta, GA, USA. ⁵New Iberia Research Center, University of Louisiana Lafayette, Lafayette, LA, USA. ⁶Yerkes National Primate Research Center, Emory University, Atlanta, GA, USA. ⁷Robert P. Apkarian Integrated Electron Microscopy Core, Emory University, Atlanta, GA, USA. ⁸Department of Pathobiology and Population Medicine, College of Veterinary Medicine, Mississippi State University, Mississippi State, MS, USA. ⁹School of Physics, Georgia Institute of Technology, Atlanta, GA, USA. ¹⁰Department of Veterinary Biosciences and Diagnostic Imaging, College of Veterinary Medicine University of Georgia, Athens, GA, USA. ¹¹School of Biological Sciences, Georgia Institute of Technology, Atlanta, GA, USA. ¹²These authors contributed equally: Laura Rotolo, Daryll Vanover, Nicholas C. Bruno. ✉e-mail: philip.j.santangelo@emory.edu

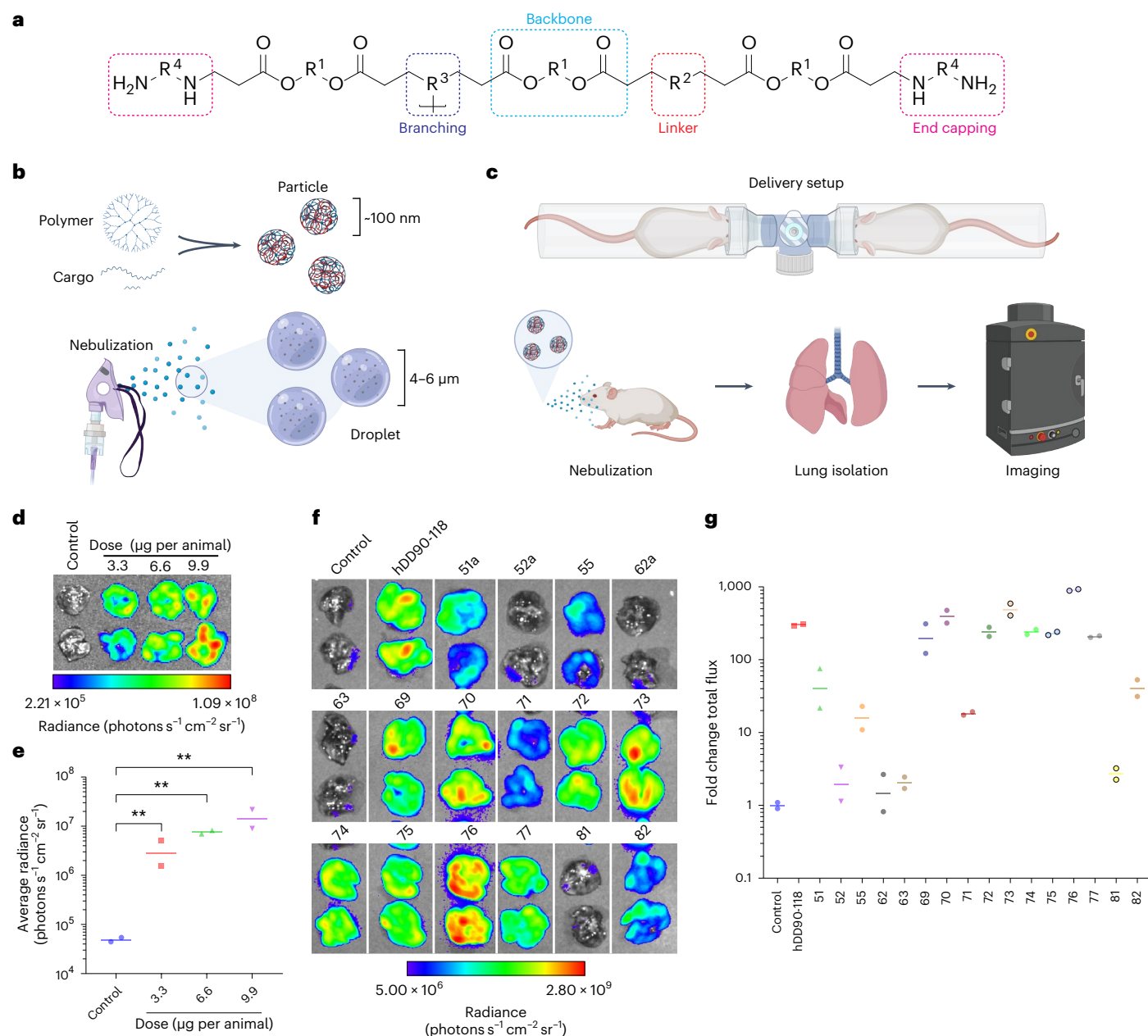


Fig. 1 | Functional screening of polymers for nebulized mRNA delivery.

a, Polymers were synthesized using one or more of four components each: a backbone, a linker component, a branching component and an end-capping structure. **b**, One or more cargo RNAs are formulated into polyplexes approximately 100–200 nm in diameter. This colloidal mixture is nebulized, creating droplets of 4–6 μm, and inhaled. **c**, Polymer screening setup. Polyplexes are nebulized into mice, and lungs are isolated and analysed by luminescence. **d, e**, Bioluminescence using nose-only nebulization of mRNA-encoded aNLuc. Images (**d**) and fold change total flux (**e**) of lungs 24 h after

delivery in mice using the hDD90-118 PBAE at the indicated doses. ****** $p < 0.01$ (one-way ANOVA with multiple comparisons on log-transformed data). $n = 3$ mice per group. The bars represent the geometric mean. p values are listed in Supplementary Table 3. **f, g**, Representative polymer formulation screening results. Images (**f**) and fold change total flux (**g**) of lungs 24 h after aNLuc mRNA nebulization into mice using the indicated polymers at 5 mg kg⁻¹. $n = 2$ mice per group. Additional screens are provided in Supplementary Fig. 3 and polymer ID definition, Supplementary Table 1. p values are listed in Supplementary Table 2.

patients^{1–6}. The most prominent clinical trial to date consisted of a nebulized CF transmembrane conductance regulator mRNA (MRT5005) from Translate Bio, formulated with a lipid nanoparticle, yet failed to produce sufficient protein to improve lung function in CF patients⁷.

Poly-β-amino-esters (PBAEs) have already demonstrated protein expression via nebulizer administration to the lungs of mice with minimal observed toxicity^{8,9}. Although the prior PBAE study only focused on the expression of reporter constructs, our group recently demonstrated the use of a hyperbranched PBAE for the nebulized

delivery of mRNA-expressed clustered regularly interspaced short palindromic repeat (CRISPR)-associated protein 13 (Cas13a) along with a guide RNA¹⁰. We observed therapeutic levels of Cas13a expression and guide RNA delivery in both mice and hamsters against influenza and SARS-CoV-2, respectively.

To improve the pulmonary delivery of PBAE formulations, we used a combinatorial synthesis strategy with a low-dead-volume nebulizer-based particle screening system to assess 166 PBAEs and PBAE-containing formulations in mice. From these initial screens, we

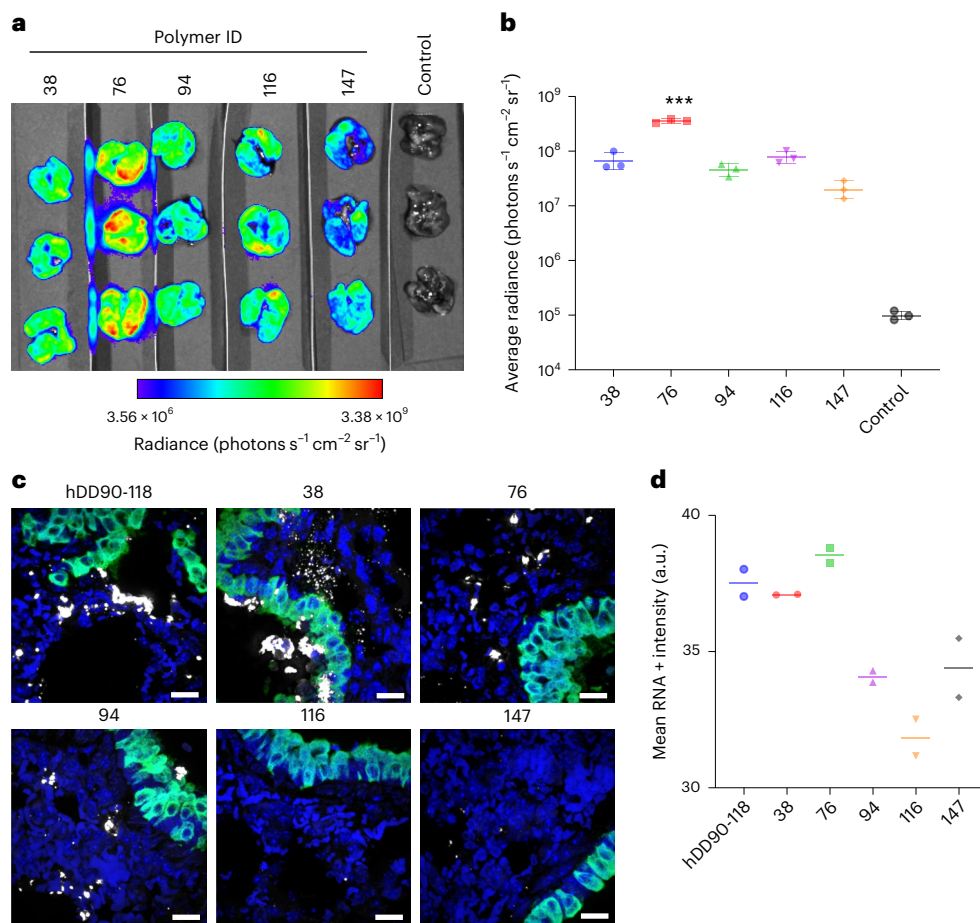


Fig. 2 | Comparison of lead polymer candidates. a, b, Luminescence measurements using the lead polymer candidates. Images (a) and fold change total flux (b) of lungs 24 h after aNLuc mRNA nebulization into mice using the indicated polymers at 5 mg kg^{-1} . *** $p < 0.001$ compared with all the other groups (one-way ANOVA with multiple comparisons on log-transformed data). The bars indicate the geometric mean \pm standard deviation (s.d.). c, Representative microscopy of mouse lungs 4 h after nebulized delivery with the indicated

polymer. FISH for aNLuc (white), *Scgb1a1* marker of airway cells (green) and nuclei stained via 4',6-diamidino-2-phenylindole (DAPI, blue). Scale bar, 15 mm. $n = 2$ mice per group. Larger lung areas are presented in Supplementary Fig. 8. d, Quantification of mean intensity of aNLuc-positive RNA granules in lungs from c. The bars represent mean. $n = 2$ mice per group. Per-cent area measurements are shown in Supplementary Fig. 9. All the p values are listed in Supplementary Table 3.

demonstrated that candidate P76, a poly- β -amino-thio-ester (PBATE) enables potent delivery of mRNA—regardless of cargo size and complexity—to mice, hamsters, ferrets, cows and rhesus macaques. P76 was found to be safe and well tolerated, with greater expression than previous nebulized PBAE candidates; it allowed for fourfold dose sparing, compared with previous nebulized PBAEs, in a Cas13a efficacy study against SARS-CoV-2 in the Syrian hamster model. This approach was also shown to be competitive with high doses of intraperitoneal-delivered neutralizing antibodies.

Functional screening of polymers for nebulized mRNA delivery

Using the hDD90-118 PBAE as the starting point, we designed a set of polymers for mRNA delivery to the respiratory track via nebulizer (Supplementary Figs. 1 and 2 and Supplementary Table 1)⁹. This set of 166 polymers were designed using a similar fundamental structure consisting of (1) diacrylate backbone electrophilic components; (2) multifunctional amines, amino alcohols and amino thiols as linear or branching nucleophilic components; and (3) diamine or aminothiol components added in excess after an initial polymer-forming step to place amine groups at the chain ends (Fig. 1a and Supplementary Fig. 1). In addition to the bisphenol glycerol diacrylate used in hDD90-118, we synthesized and tested polymers and copolymers containing

diacrylates derived from a variety of other building blocks including glycidyl ethers, xanthene dyes and steroids, as well as several methacrylate, acrylamide and epoxide derivatives. We also explored the use of a variety of linkers and branching monomers, including amino acids and cholesterol amines.

These polymers were exclusively tested in pH 5.0 sodium acetate buffer to retain the protonation of the polymer, facilitating RNA binding. When delivered via a vibrating mesh nebulizer, the nanoparticle colloid is aerosolized, with a droplet diameter of the order of 4–6 μm for enhanced drug delivery to the deep lung (Fig. 1b)^{11,12}.

To perform a functional screen, polyplexes of each candidate polymer with mRNA encoding a glycosylphosphatidylinositol-anchored nanoluciferase (aNLuc) reporter were formulated; hDD90-118 was used as a positive control¹⁰. Polyplexes containing aNLuc mRNA were then tested using a vibrating mesh nebulizer attached to a custom nose-only apparatus, evaluating functional in vivo delivery via nanoluciferase expression (Fig. 1c). Our nose-only nebulizer apparatus design minimizes the dead volume (the space between the nebulizer outlet and inhaling region of the animals), allowing for doses as low as 0.165 mg kg^{-1} (3.3 μg per mouse) of aNLuc mRNA (Fig. 1d, e). In addition, the apparatus exhibited minimal animal-to-animal variability in expression, allowing for the use of only two animals per formulation.

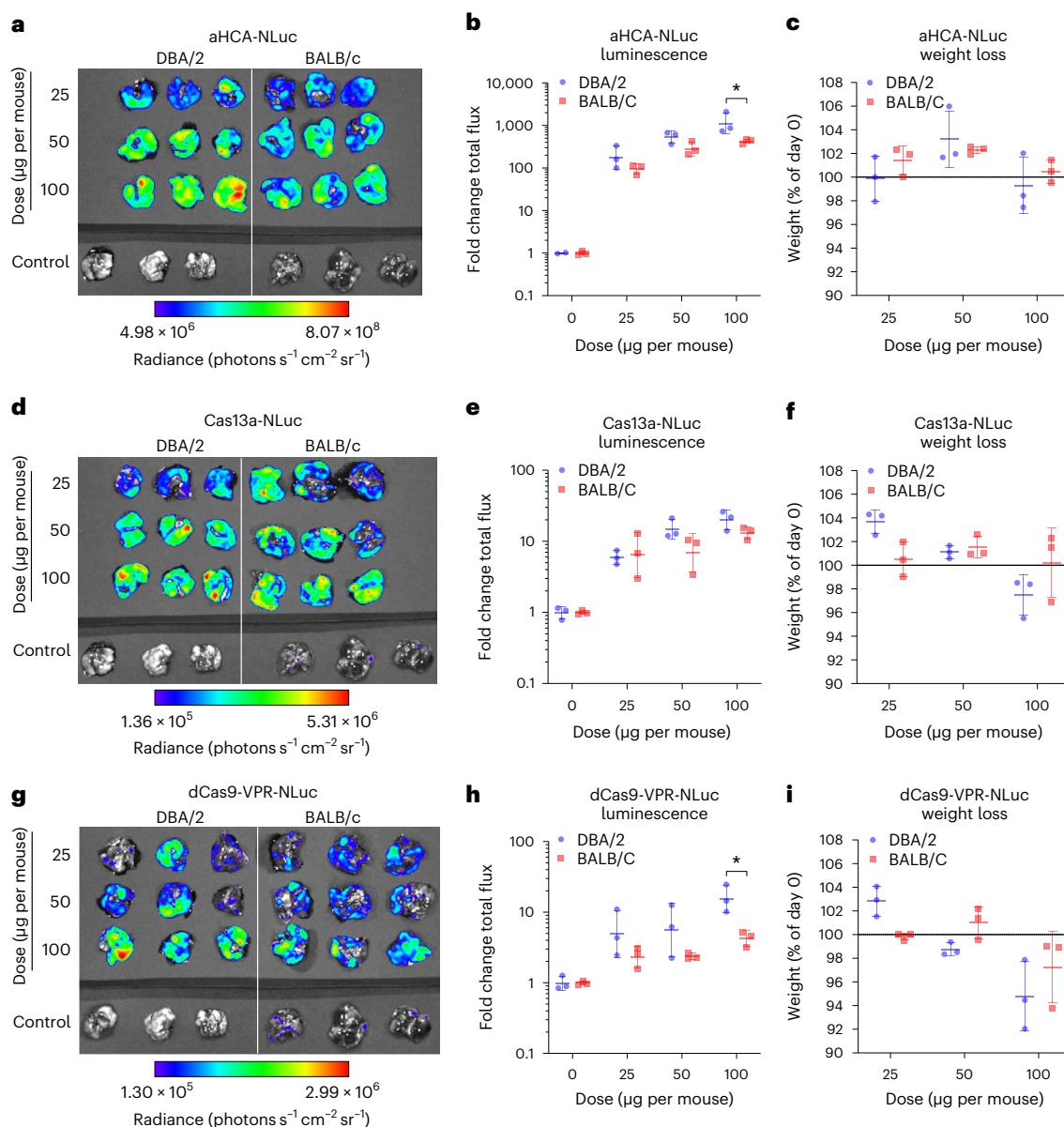


Fig. 3 | P76 delivers cargo of any size to the lungs of mice with minimal toxicity. **a–i**, P76 delivers a large range of cargo lengths in DBA/2 and BALB/c mice. The lungs were evaluated at 24 h post transfection using the indicated doses of mRNA or mRNA and crRNA formulated with P76. Images (**a**), fold change total flux (**b**) and weight change (**c**) in mice transfected with aHCA-NLuc mRNA. Images (**d**), fold change total flux (**e**) and weight change (**f**) in mice transfected

with Cas13a-NLuc mRNA and crRNA. Images (**g**), fold change total flux (**h**) and weight change (**i**) in mice transfected with dCas9-VPR-NLuc mRNA and crRNA. $n = 3$ mice per group. $*p < 0.05$ (two-way ANOVA with multiple comparisons on log-transformed data). For the luminescence data, bars indicate geometric mean \pm s.d. For weight data, bars indicate mean \pm s.d. The horizontal line represents no weight change. All the p values are listed in Supplementary Table 3.

Five lead candidate polymers (P38, P76, P94, P116 and P147) emerged from the initial screen with expression as high or higher than hDD90-118 (Fig. 1f, g, Supplementary Table 2 and Supplementary Figs. 3–6). In some of these lead polymers, we incorporated cysteamine or 1,2-ethanedithiol as the nucleophilic main-chain building blocks, which add onto acrylates much faster than amines. P76, which incorporated the dithiol and was designated as a PBATE, exhibited 3.02-fold higher expression compared with hDD90-118. The dithiol is particularly interesting, since small amounts react quickly with bis(acrylates), creating macromonomer or block-oligomer-like components in situ. In addition, nuclear magnetic resonance (NMR) analysis of hDD90-118 and the five lead candidate polymers revealed the presence of peaks in the 8.00–8.15 ppm range, unexpected for the previously reported

composition (Supplementary Fig. 7)⁹. Given the described reaction conditions (heating in *N,N*-dimethylformamide (DMF) solvent at 90 °C for 48 h), *N*-formylation is probable, since DMF is known to be a potential donor of the formyl group^{13–18}. The carbonyl groups derived from the solvent were confirmed by the preparation of hDD90-118 in the presence of ¹³C-enriched DMF (Supplementary Fig. 7). The delivery of reporter mRNA to mice lungs using hDD90-118 made in a different solvent (*N,N*-dimethylpropyleneurea, polymer 98) was much lower than hDD90-118 made using DMF, suggesting that *N*-formylation may be a key attribute (Supplementary Fig. 3). Overall, these results demonstrate that our nebulizer apparatus, when used in conjunction with a sensitive luminescent reporter construct, is ideal for discovering lead polymer formulations that potentially deliver mRNA in vivo.

Chemical analysis and performance of lead candidate polymers

To identify a lead formulation, we compared P38, P76, P94, P116 and P147 using a variety of assays. We first compared the expression of a 5 mg kg⁻¹ dose of aNLuc mRNA formulated with the lead polymers in the lungs of mice (Fig. 2a). Delivery with P76 PBATE resulted in a geometric mean lung radiance of 3.58×10^8 photons s⁻¹ cm⁻² sr⁻¹, significantly higher (by 5.46, 7.88, 4.63 and 18.12 times) than P38, P94, P116 and P147, respectively (Fig. 2b). We then analysed the distribution of mRNA cargo delivered by our lead polymers along with hDD90-118 in the lungs of mice. Fluorescent in situ hybridization (FISH) microscopy revealed that P38, P76, P94 and hDD90-118 delivered mRNA to the lungs, with P38 and P94 delivery resulting in some deposition of RNA in the airways, whereas P76 and hDD90-118 delivery produced more alveolar RNA signals (Fig. 2c and Supplementary Fig. 8). Quantification of the FISH signal revealed that the per cent of RNA-positive lung area does not strongly correlate with the expression (Supplementary Fig. 9). However, P76, P38 and hDD90-118 formulations resulted in a slight increase in the mean intensity of RNA-positive regions, correlating with a higher aNLuc expression (Fig. 2d).

All the particles exhibited highly positive surface zeta potentials and favourable diameters before and after nebulization (Supplementary Text 1 and Supplementary Figs. 10 and 11). In addition, molecular dynamics simulations were performed to begin to investigate the interaction of P76 with mRNA (Supplementary Text 1 and Supplementary Fig. 10). Finally, we measured a wide range of mass ratios, between 10:1 and 100:1, finding minimal changes in the expression of aNLuc mRNA, with the exception of the 10:1 ratio (Supplementary Fig. 12). Thus, we elected to keep the 50:1 mass ratio that was previously used with hDD90-118 (ref. 9).

Nebulized delivery of a variety of mRNA cargos using P76

We next attempted to determine the ability of P76 to deliver RNA cargos of various lengths and complexity to the lungs of mice. We delivered mRNA encoding an immunoglobulin G antibody (light-chain mRNA length, 1,890 nucleotides (nt); heavy-chain mRNA length with encoded glycosylphosphatidylinositol anchor, 2,180 nt), called aHCA, with no target in non-human species LbuCas13a (4,719 nt)—an activatable RNase—or the gene activator dCas9-VPR (~7,055 nt). For both Cas13a and dCas9-VPR, we also included a CRISPR RNA (crRNA) of 60 nt for Cas13a and 100 nt for dCas9-VPR, to simulate a CRISPR drug. To assess the immunoglobulin G expression, we used an mRNA-encoded light chain fused to the NLuc protein (aHCA-NLuc), whereas for the Cas13a and dCas9-VPR constructs, the NLuc reporter sequence was downstream of an encoded P2A cleavage site¹⁹. We also investigated the difference in expression using P76 between BALB/c and DBA/2 mice strains since strain-dependent differences in transfection efficiency have been previously reported²⁰.

First, when mRNA encoding aHCA-NLuc was administered via nebulizer, DBA/2 mice displayed an increase in the geometric mean signal fold change compared with BALB/c mice at the tested dosages

of 1.25, 2.50 and 5.00 mg kg⁻¹ (Fig. 3a,b). This increase in signal was 2.10 times higher in the DBA/2 mice. Neither mouse strain displayed any significant weight change after 24 h, a clinical metric of general health, at any of the tested dosages of aHCA-NLuc mRNA (Fig. 3c). When mice were delivered the same dosages above of Cas13a-NLuc along with crRNA, DBA/2 mice produced a signal 1.52 times higher than BALB/c on average, resulting in a small but measurable drop in weight that increased according to dose (Fig. 3d–f). Finally, dCas9-VPR-NLuc mRNA delivered via P76 to DBA/2 mice exhibited a signal 2.69 times higher than BALB/c mice on average (Fig. 3g,h). Similar to the Cas13a-NLuc results, mice who received dCas9-VPR-NLuc mRNA, delivered with crRNA, did elicit a small but measurable drop in weight that increased according to dose (Fig. 3i). Overall, these results demonstrate that P76 can deliver cargo across a wide range of sizes and confirmed that DBA/2 mice consistently demonstrated a slightly higher expression than BALB/c mice. The slight increase in protein expression in the DBA/2 mice is probably due to a combination of increased inspiratory duty cycle of 19% over the BALB/c strain and inter-strain differences in lung anatomy^{21,22}.

To confirm that P76 efficiently delivers mRNA of various lengths, we delivered 25 µg of either aNLuc (1,298 nt) or Cas13-NLuc (4,898 nt) to the lungs of mice via the nebulizer and analysed the amount of RNA delivered to the lungs by a quantitative polymerase chain reaction (PCR). We measured no statistical difference in the mass of delivered mRNA despite the 3.77 times difference in mRNA length, indicating that P76 delivers cargos of different lengths with similar efficiency (Supplementary Fig. 13). Considering that (1) the increased size of the Cas13 and VPR constructs results in fewer RNA copies delivered at the same dosage compared with the anchored antibody construct, (2) the membrane anchor retains the antibody in the tissue and increases the NLuc signal^{2,19,23} and (3) the 80–95% efficiency loss of NLuc expression due to the P2A cleavage site²⁴, the signal observed in mice lungs transfected with the Cas13 and VPR constructs has similar expression to the antibody construct when the above factors are taken into account.

Nebulized P76 delivery is minimally toxic

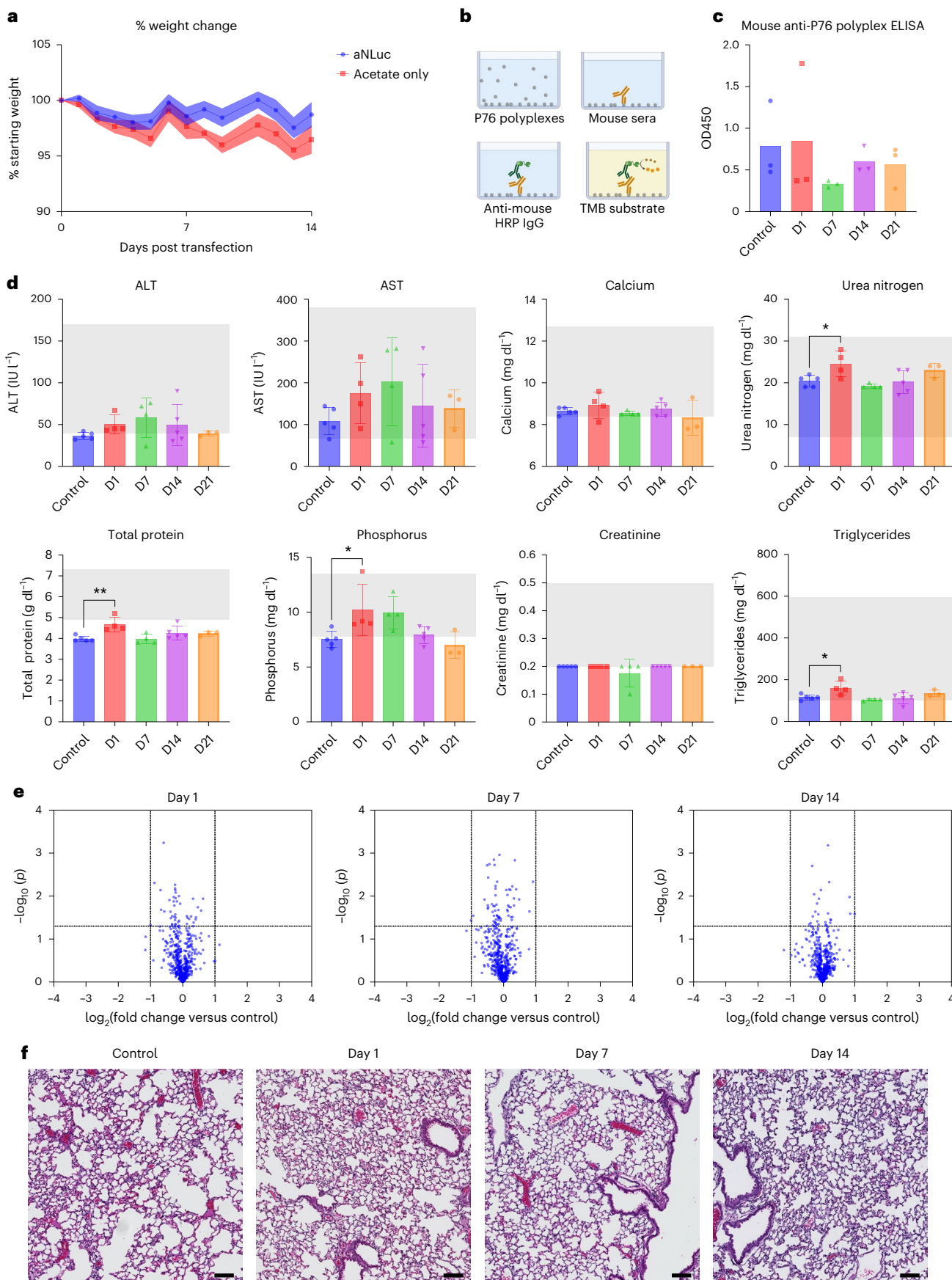
We then more closely examined the toxicological effects and biodistribution of nebulized P76 delivery to mice. We delivered 1.25 mg kg⁻¹ of P76-formulated aNLuc mRNA and analysed the (1) weight changes, (2) serum anti-P76 polyplex antibody levels, (3) complete blood chemistry, (4) lung-tissue-level differential gene expression and (5) histopathology over a 21 day period post exposure. First, over the first 14 days, we observed no significant difference in weights between the P76-treated and untreated animals (Fig. 4a). Second, we analysed the potential immunological responses by investigating whether treated animals developed anti-P76 polyplex antibodies (Fig. 4b). None of the serum, out to 21 days, had any detectable levels of antibodies over the assay background signal in the control group (Fig. 4c). Next, we analysed the complete blood chemistry metrics (Fig. 4d). Although the day 1 levels of total protein, urea nitrogen, phosphorus and triglycerides were elevated compared with untreated animals, all the metrics at all the time points fell within or below the 95% confidence interval

Fig. 4 | Nebulized P76 delivery is minimally toxic. aNLuc mRNA was delivered via P76 at 1.25 mg kg⁻¹. Acetate buffer was delivered to the control group. Mice were sacrificed at days 1, 7, 14 and 21 for terminal blood and tissue collection. For each time point, $n = 6$ mice weights were measured. At the indicated days, blood draws were performed on all the mice; $n = 3$ mice lungs were used for NanoString analysis and $n = 3$ mice lungs were used for histopathology analysis. **a**, Weights as a percentage of starting weight. The error bands represent \pm standard error of the mean (s.e.m.). **b**, Schematic of enzyme-linked immunoassay (ELISA) to detect mouse anti-P76 polyplex antibody responses at days 1, 7, 14 and 21. Horseradish peroxidase (HRP); 3,3',5,5'-Tetramethylbenzidine (TMB). **c**, Mouse anti-P76 polyplex antibodies were detected via ELISA. The bars represent mean optical density at 450 nm (OD450). No significant difference was measured by one-way

ANOVA ($p = 0.6450$). **d**, Complete blood chemistry metrics. * $p < 0.05$, ** $p < 0.01$ (one-way ANOVA with Dunnett's multiple comparisons). The grey regions represent 95% confidence interval of naïve mice from Charles River Laboratories. Samples with insufficient sera or excessive haemolysis were excluded from the analysis. The bars in all the graphs indicate mean \pm s.d. **e**, Differential gene expression of 561 inflammatory genes measured by NanoString analysis of the indicated time points versus the control. The horizontal line represents $p = 0.05$ (two-tailed t -test on log-transformed normalized data) and the vertical lines indicate fold changes of ± 2 . **f**, Representative H&E-stained lung sections from mice at the indicated time point. Scale bar, 100 µm. $n = 2$ mice per group. All the p values are listed in Supplementary Table 3.

of these measures for normal animals, as reported by Charles River Laboratories. Next, we investigated changes in 561 immune marker genes within mouse lungs 1, 7 and 14 days after a single exposure to

P76 polyplexes (Fig. 4e). No significantly differentially expressed genes were detected at any time point. This corroborates previous reports of modified mRNA transfection in mice and demonstrates minimal



immunological effects of the polymer²⁵. Next, we assessed lung tissue pathology at 1, 7 and 14 days post P76 polyplex exposure. No animals exhibited any evidence of necrosis, oedema, inflammation or other lesions (Fig. 4f). Finally, we observed no detectable luminescence in the kidneys, heart, spleen, paraaortic lymph node or liver of mice that were delivered 5 mg kg⁻¹ of aNLuc mRNA formulated via P76 (Supplementary Fig. 14). Together, these data indicate neither pathology nor differential gene expression after P76 polyplex delivery via the nebulizer, and that functional particle delivery is restricted to the lungs.

P76 delivers mRNA across species with minimal toxicity

Although testing mRNA vehicles in mice is critical for early stage pharmaceutical testing, preclinical studies require testing lead candidates in a variety of species for efficacy and toxicology studies. We first compared the delivery of P76 across mice, hamsters and ferrets at a constant 0.3 mg kg⁻¹ dose of aNLuc mRNA. Interestingly, the average radiance increased as the animal size increased (Fig. 5a–d). Specifically, the geometric mean of average radiance was 3.3 and 8.5 times higher in the hamster and ferret lungs, respectively, compared with mouse lungs, probably due to lower tidal volumes in smaller animals (Fig. 5b,c). Overall, these data support the use of P76 in mice, hamsters and ferrets as an efficient vehicle for mRNA therapeutic delivery.

Next, to evaluate the delivery in a large animal, we assessed the delivery of P76-formulated aNLuc mRNA in an adolescent cow (approximately 113 kg). Cows of this size are an excellent model of human and bovine respiratory syncytial virus²⁶. On nebulizer delivery of 0.03 mg kg⁻¹ of aNLuc mRNA, we observed luminescence across the lung tissue, with peak radiances greater than 10⁷ photons s⁻¹ cm⁻² sr⁻¹ (Fig. 5e). The 0.03 mg kg⁻¹ dose was chosen to limit the nebulization time as we employed the same Aerogen nebulizer used for the rodents. Finally, delivery via P76 resulted in aNLuc expression even within larger cartilaginous airways, indicating broad delivery targets in the lungs (Supplementary Fig. 15).

As non-human primates are often predictive of therapeutic and disease responses in humans, we performed a test of the nebulized delivery of aNLuc mRNA via P76 in rhesus macaques. Compared with the control animal, P76 resulted in 116- and 5,610-fold increase in the average radiance over control tissue from 4 to 24 h post transfection (Fig. 5f,g). Like the bovine results above, the visceral pleura blocked luminescent substrate delivery to alveolar tissue in some regions. Finally, P76 efficiently delivered mRNA to human cell lines (Supplementary Fig. 16). The high expression of the aNLuc reporter in both bovine and macaque lungs, as well as in human cells, strongly supports the use of P76 in preclinical research.

We next evaluated a dose response of the more relevant mRNA reporter constructs in the ferret to assess the expression in larger species. First, we tested doses of 0.03, 0.10 and 0.30 mg kg⁻¹ of aHCA-NLuc mRNA, finding a significant, linear increase in the average radiance with increasing dose ($R^2 = 0.893$, $p = 0.0044$) (Fig. 5h,i). Similarly, we observed a linear dose response when delivering the same dosages of Cas13a-NLuc mRNA along with crRNA ($R^2 = 0.793$, $p = 0.0173$) (Fig. 5j,k).

Fig. 5 | P76 delivers RNA cargo in a species-agnostic manner with minimal toxicity. a–d, P76 efficiently delivers mRNA to mouse, hamster and ferret lungs. Images (a), average radiance (b), total area (c) and total flux (d) of lungs at 24 h post transfection of aNLuc mRNA at 0.3 mg kg⁻¹ using P76. $n = 2$ animals per species. The bars indicate geometric mean (average radiance and total flux) or mean (weight). e, Luminescence image of a section of the left diaphragmatic lung of cow 24 h after transfection of aNLuc mRNA at 0.03 mg kg⁻¹ using P76. Additional images are provided in Supplementary Fig. 15. f,g, Nebulized P76 formulations deliver RNA throughout the lung lobes of rhesus macaques. Images (f) and average radiance (g) of lungs at 4 and 24 h post transfection of aNLuc mRNA at 0.3 mg kg⁻¹ using P76. The control animal was untreated. $n = 1$ per group. h–k, P76 delivers RNA cargo in a linear dose-dependent manner with minimal toxicity. Images (h) and average radiance (i) of ferret lungs 24 h post

transfection of aHCA-NLuc mRNA at the indicated doses. Images (j) and average radiance (k) of ferret lungs 24 h post transfection of Cas13-NLuc mRNA at the indicated doses. The blue lines represent linear regression, and the dotted line represents the average radiance of the control animal. $n = 2$ ferrets per group.

These data provide strong evidence for the potent delivery of therapeutic mRNA cargos in the larger ferret model, even at lower doses, supporting future influenza therapeutic trials in challenge experiments. We next assessed the biodistribution of P76-mediated RNA delivery at the cellular level in the larger animal models using FISH. In the ferret, we observed well-distributed RNA signal of both aHCA-NLuc and Cas13a-NLuc mRNAs, indicating that the mRNA length does not substantially impact the distribution of delivery in the lungs (Fig. 5l). This trend continued in the larger macaque lungs, with aNLuc mRNA appearing well dispersed throughout the tissue (Fig. 5m and Supplementary Fig. 17). Given the smaller size and thus higher number of aNLuc mRNA molecules delivered to the lungs (compared with Cas13a-NLuc mRNA), the RNA signal in the macaque appeared much stronger than in the ferrets, despite the equal dosage. In both species, mRNA delivered via P76 primarily targeted cells in the alveolar space rather than airway cells.

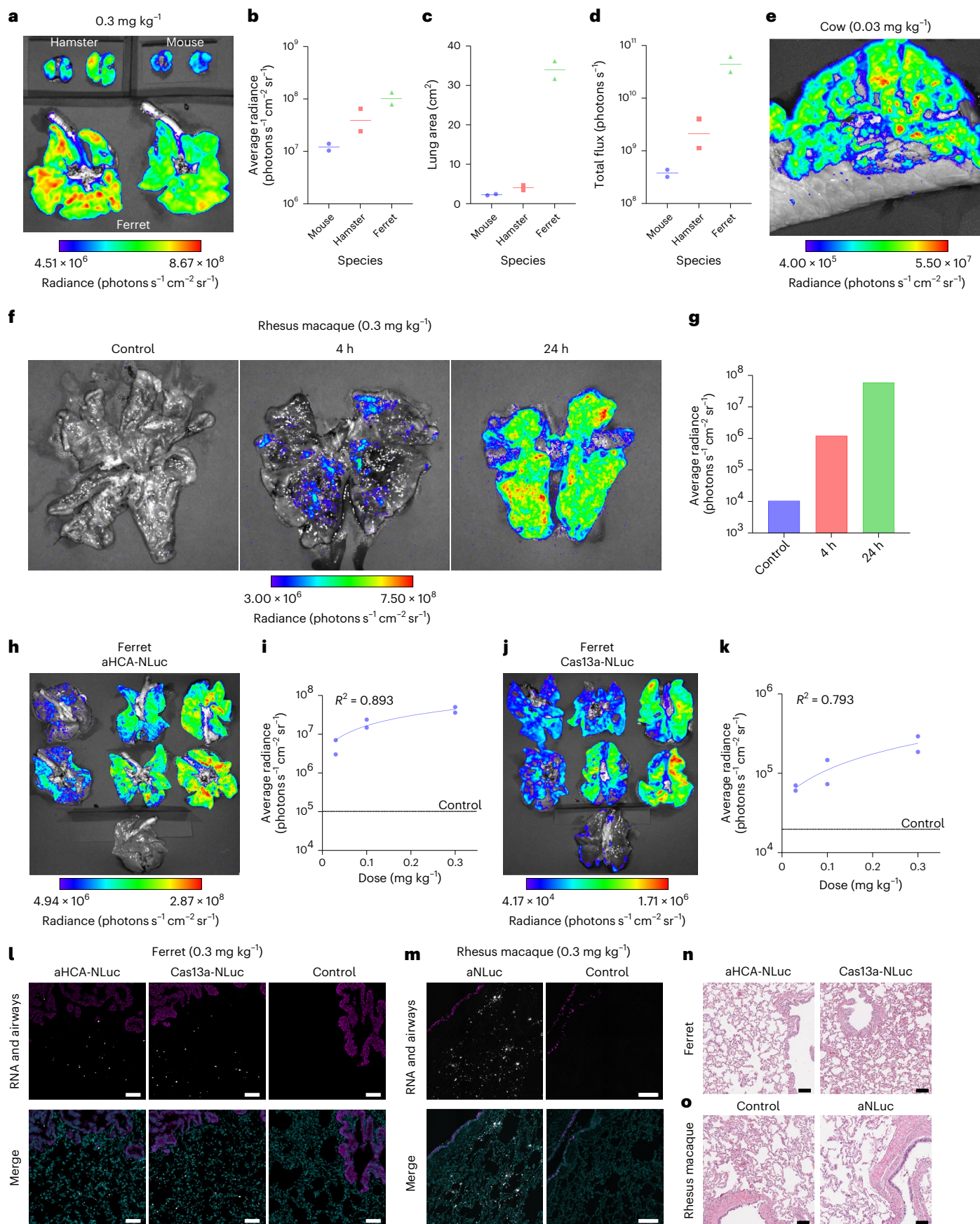
Initial toxicity assessment in both ferret and macaque yielded no significant findings by the histological analysis of the treated lungs at 24 h with a 0.3 mg kg⁻¹ dose (Fig. 5n,o). The analysis of serum before and after dosing in the macaques revealed minimal increases in serum cytokine levels (Supplementary Table 5). Last, haematology and blood chemistry analyses revealed only minor changes in most metrics, with all but one remaining within normal levels for macaques (Supplementary Tables 6 and 7). Taken together, these data strongly support the nebulized use of P76 for high mRNA delivery with minimal toxicity in future preclinical applications.

P76 delivers mRNA and guide at therapeutic levels

Finally, we compared the therapeutic efficacy of P76 with PBAE hDD90-118. First, the Cas13a-NLuc reporter mRNA was delivered via nebulizer at 1.25 mg kg⁻¹ to hamsters, finding that P76 delivery resulted in a 2.05-fold increase in signal (Fig. 6a). However, when a crRNA was delivered alongside the Cas13a-NLuc mRNA, the P76 formulation produced 19.1, 2.9, and 16.4 times more signal when delivered at 0.310, 0.625 and 1.250 mg kg⁻¹, respectively, compared with hDD90-118 (Fig. 6b,c). The increase in Cas13-NLuc expression was not due to a difference in mRNA and crRNA binding between P76 and hDD90-118 (Supplementary Text 3 and Supplementary Fig. 18).

Next, we tested the therapeutic efficacy of P76 formulations in a SARS-CoV-2 challenge in the hamster model. Hamsters were treated with LbuCas13a mRNA alongside our previously validated anti-SARS-CoV-2 crRNA, N3.2, with a P76 or hDD90-118 formulation and intranasally infected 20 h later with 1,000 plaque-forming units (PFU) of the WA-1 strain of live SARS-CoV-2 (Fig. 6d)¹⁰. Hamsters were weighed daily as a measure of general health, and when both P76 and hDD90-118 formulations were delivered at 0.5 mg kg⁻¹, only the P76 formulation prevented differential weight loss due to SARS-CoV-2 challenge over 5 days (Fig. 6e). Critically, the animals treated with a 0.5 mg kg⁻¹ dose of P76-formulated Cas13 mRNA with N3.2 crRNA gained a significant amount of body weight by day 5 compared with both virus-only control group and 0.5 mg kg⁻¹ hDD90-118 formulation (Fig. 6f). These data suggest that P76 is significantly more efficient at delivering the Cas13

transfection of aHCA-NLuc mRNA at the indicated doses. Images (j) and average radiance (k) of ferret lungs 24 h post transfection of Cas13-NLuc mRNA at the indicated doses. The blue lines represent linear regression, and the dotted line represents the average radiance of the control animal. $n = 2$ ferrets per group. l,m, Representative FISH microscopy of ferret (l) and macaque (m) lungs 4 h post transfection at the indicated dose of RNA cargo (white) using P76. *Scgb1a1* and *Foxj1* airway markers (magenta) and nuclei (DAPI, cyan) for context. Scale bars, 200 μ m (l) and 60 μ m (m). $n = 2$ ferrets per group (l) or $n = 1$ macaque per group (m). The full section images of macaque lungs are shown in Supplementary Fig. 17. n, Histology of ferret lungs 24 h post transfection of 0.3 mg kg⁻¹ of the indicated RNA cargo using P76. $n = 2$ ferrets per group. o, Histology of macaque lungs 24 h post transfection of 0.3 mg kg⁻¹ of aNLuc mRNA using P76. Scale bars, 100 μ m. $n = 1$ macaque per group.



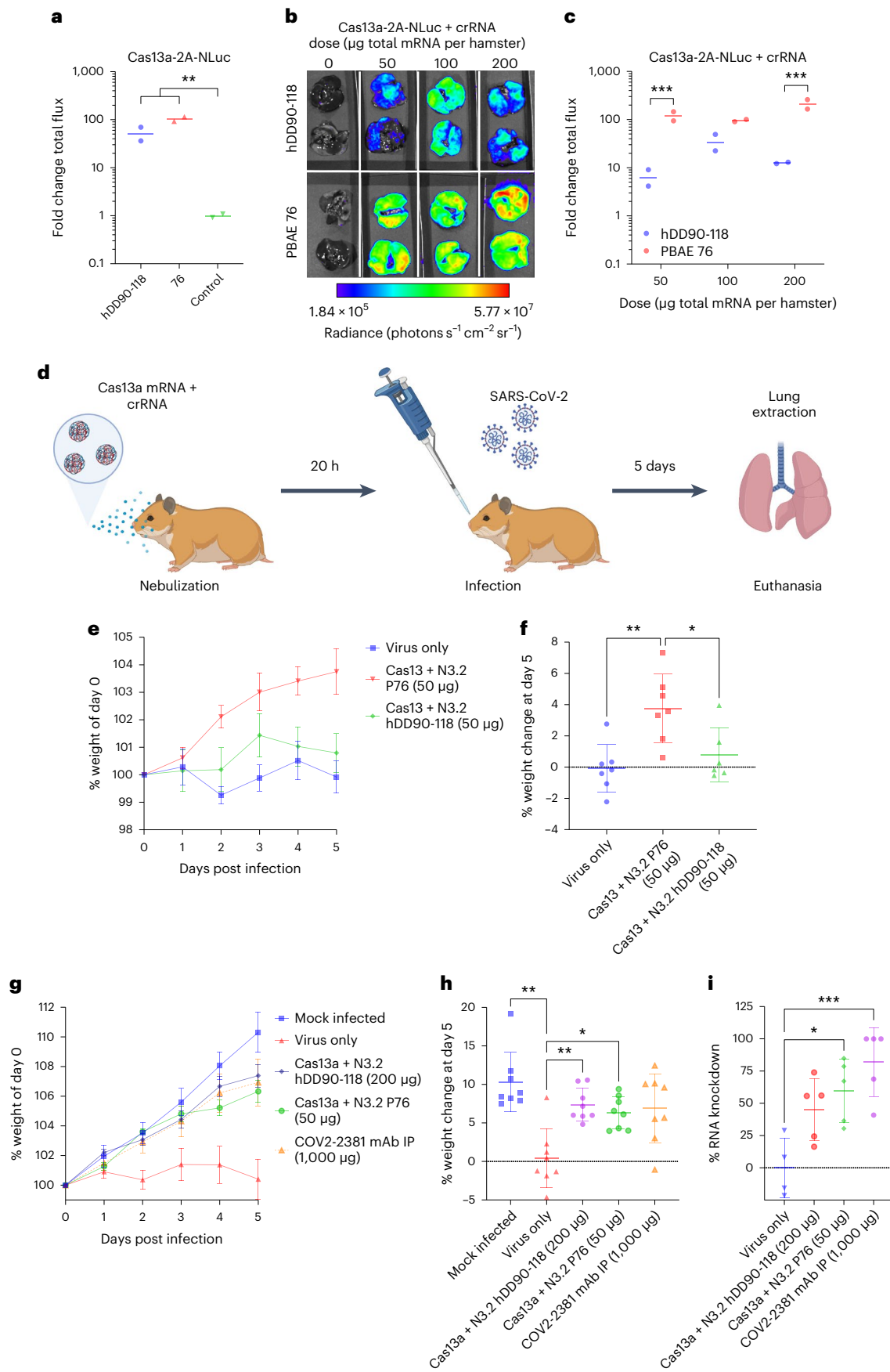


Fig. 6 | P76 efficiently delivers mRNA and crRNA and prevents SARS-CoV-2 infection in hamsters. **a**, Nebulized P76 formulations are more efficient than hDD90-118. The quantification of hamster lung luminescence at 24 h post transfection of 1.25 mg kg⁻¹ of Cas13a-NLuc mRNA. The bars represent geometric mean \pm s.d. $n = 2$. ** $p < 0.01$ (one-way ANOVA with Dunnett's multiple comparisons on log-transformed data) **b,c**, Nebulized P76 formulations are more efficient than hDD90-118 at delivering RNA cargo of different lengths. Images (**b**) and fold change total flux (**c**) of hamster lungs 24 h after delivery of the indicated total dose of Cas13-NLuc mRNA and crRNA. The bars represent geometric mean \pm s.d. $n = 2$. *** $p < 0.001$ (one-way ANOVA with Šidák's multiple comparisons on log-transformed data). **d–i**, P76 delivery of Cas13 mRNA along with N3.2 guide prevents SARS-CoV-2 infection in the hamster model. **d**, Hamsters were treated with either nebulized P76 or hDD90-118-formulated Cas13 mRNA and crRNA.

20 h later, the hamsters were intranasally inoculated with 10³ PFU of WA-1 SARS-CoV-2. The hamsters were euthanized on day 5 and the lungs were extracted and processed for viral load quantification. $n = 8$ hamsters per group. **e**, Per-cent normalized hamster weight over time. The symbols and error bars represent mean and per-cent weight \pm s.e.m., respectively. **f**, Per-cent hamster weight at day 5 post infection. The bars represent mean \pm s.d. **g**, Per-cent normalized hamster weight over time. The symbols and error bars represent mean and per-cent weight \pm s.e.m., respectively. **h**, Per-cent hamster weight at day 5 post infection. The bars represent mean \pm s.d. **i**, Per-cent knockdown of SARS-CoV-2 RNA in the lung at day 5 post infection. The bars represent mean \pm s.d. * $p < 0.05$, ** $p < 0.01$, *** $p < 0.001$ (one-way ANOVA with Dunnett's multiple comparisons). $n = 4–5$ per group. All the p values are listed in Supplementary Table 3.

mRNA and crRNA than hDD90-118, consistent with the luminescence data (Fig. 6c).

To further validate the potency of P76 formulations, we performed the same study with the 0.5 mg kg⁻¹ P76 formulation and an increased dose of 2.0 mg kg⁻¹ of the hDD90-118 formulation. We also compared these mRNA-based formulations with one group of hamsters that was treated via intraperitoneal administration with 10 mg kg⁻¹ of the potent neutralizing monoclonal antibody, COV2-2381, as a gold-standard control²⁷. One group of hamsters was mock infected, whereas another group was untreated and infected as a negative and positive control, respectively. We found that the 0.5 mg kg⁻¹ Cas13a mRNA dose using P76 performed as well as both 2.0 mg kg⁻¹ dose using hDD90-118 and 10.0 mg kg⁻¹ dose of COV2-2381, with all the treated hamsters gaining 6.88% body weight on average over 5 days (Fig. 6g). Weight change at day 5 was only significantly improved by the hDD90-118 and P76 formulations (Fig. 6h), and there was no significant difference among the treated groups. Interestingly, SARS-CoV-2 RNA knockdown in the lungs was only significantly reduced by 59.5% and 81.9%, compared with the virus-only group, at day 5 in hamsters treated with either P76-formulated Cas13a or COV2-2381, respectively (Fig. 6i), but there was no significant difference between the treated groups.

Outlook

Efficient pulmonary delivery of mRNA has the potential to support a variety of pharmaceutical development programs ranging from antivirals and inhalable vaccines to CF treatment^{10,28,29}. To date, the majority of pulmonary-targeted nucleic acid vehicles have been given systemically. Although the recently reported PBAE hDD90-118 produces a strong expression of mRNA in mice, it was not capable of simultaneously delivering a crRNA without reducing the expression of the mRNA-encoded protein.

We prepared and screened 166 PBAE and PBAE-containing polymers, identifying P76 as a highly efficient vehicle for mRNA delivery via nebulizer. We demonstrated that the P76 PBATE can deliver mRNA to two mice strains, hamsters, ferrets, cows and rhesus macaques, exhibiting the species-agnostic efficacy of this polymer. Furthermore, we demonstrated that delivery in larger species is more efficient, probably through a better matching of their tidal volume and droplet size generated by the nebulizer as well as the airway and airspace sizes within the lungs. Importantly, the incorporation of thiols allowed P76 to efficiently codeliver short crRNAs with long mRNAs, dramatically increasing the utility of the polymer for any CRISPR-based therapeutic candidate. These properties allowed for a four times lower dose in a SARS-CoV-2 challenge in a hamster model using P76-delivered Cas13a mRNA compared with the previously reported PBAE, with similar efficacy to the gold standard of systemic neutralizing antibody treatment. Critically, we demonstrated the minimal toxicity of P76 formulations in mice, ferrets and macaques. Together, the PBATE P76 represents a substantial step forward for polymeric nanoparticle formulations, enabling future inhalable nucleic acid therapeutics.

Online content

Any methods, additional references, Nature Portfolio reporting summaries, source data, extended data, supplementary information, acknowledgements, peer review information; details of author contributions and competing interests; and statements of data and code availability are available at <https://doi.org/10.1038/s41563-022-01404-0>.

References

- Pardi, N. et al. Expression kinetics of nucleoside-modified mRNA delivered in lipid nanoparticles to mice by various routes. *J. Control. Release* **217**, 345–351 (2015).
- Tiwari, P. M. et al. Engineered mRNA-expressed antibodies prevent respiratory syncytial virus infection. *Nat. Commun.* **9**, 3999 (2018).
- Qiu, Y. et al. Effective mRNA pulmonary delivery by dry powder formulation of PEGylated synthetic KL4 peptide. *J. Control. Release* **314**, 102–115 (2019).
- Lokugamage, M. P. et al. Optimization of lipid nanoparticles for the delivery of nebulized therapeutic mRNA to the lungs. *Nat. Biomed. Eng.* **5**, 1059–1068 (2021).
- Chollet, P., Favrot, M. C., Hurbin, A. & Coll, J.-L. Side-effects of a systemic injection of linear polyethylenimine–DNA complexes. *J. Gene Med.* **4**, 84–91 (2002).
- Wen, Y. et al. A biodegradable low molecular weight polyethylenimine derivative as low toxicity and efficient gene vector. *Bioconjugate Chem.* **20**, 322–332 (2009).
- Translate Bio announces results from second interim data analysis from ongoing phase 1/2 clinical trial of MRT5005 in patients with cystic fibrosis (CF). <https://investors.translate.bio/news-releases/news-release-details/translate-bio-announces-results-second-interim-data-analysis/> (2021).
- Kaczmarek, J. C. et al. Polymer-lipid nanoparticles for systemic delivery of mRNA to the lungs. *Angew. Chem. Int. Ed.* **55**, 13808–13812 (2016).
- Patel, A. K. et al. Inhaled nanoformulated mRNA polyplexes for protein production in lung epithelium. *Adv. Mater.* **31**, 1805116 (2019).
- Blanchard, E. L. et al. Treatment of influenza and SARS-CoV-2 infections via mRNA-encoded Cas13a in rodents. *Nat. Biotechnol.* **39**, 717–726 (2021).
- Martini, V. et al. Distribution of droplets and immune responses after aerosol and intra-nasal delivery of influenza virus to the respiratory tract of pigs. *Front. Immunol.* **11**, 594470 (2020).
- Samuel, J. & Smaldone, G. C. Maximizing deep lung deposition in healthy and fibrotic subjects during jet nebulization. *J. Aerosol Med. Pulm. Drug Deliv.* **33**, 108–115 (2020).
- Suchý, M., Elmeirik, A. A. H. & Hudson, R. H. E. A remarkably simple protocol for the *N*-formylation of amino acid esters and primary amines. *Org. Lett.* **13**, 3952–3955 (2011).
- Yang, D.-S. & Jeon, H.-B. Convenient *N*-formylation of amines in dimethylformamide with methyl benzoate under microwave irradiation. *Bull. Korean Chem. Soc.* **31**, 1424–1426 (2010).

15. Sonawane, R. B., Rasal, N. K., Bhange, D. S. & Jagtap, S. V. Copper(II) catalyzed *N*-formylation and *N*-acylation of aromatic, aliphatic, and heterocyclic amines and a preventive study in the C-N cross coupling of amines with aryl halides. *ChemCatChem* **10**, 3907–3913 (2018).
16. Tan, Z., Li, Z., Ma, Y., Qin, J. & Yu, C. Potassium *tert*-butoxide prompted highly efficient transamidation and its coordination radical mechanism. *Eur. J. Org. Chem.* **2019**, 4538–4545 (2019).
17. Sakurai, M., Kawakami, R. & Kihara, N. TBSOTf-promoted versatile *N*-formylation using DMF at room temperature. *Tetrahedron Lett.* **60**, 1291–1294 (2019).
18. Wang, Y. et al. Transformylating amine with DMF to formamide over CeO₂ catalyst. *Chem. Commun.* **50**, 2438–2441 (2014).
19. Lindsay, K. E. et al. Aerosol delivery of synthetic mRNA to vaginal mucosa leads to durable expression of broadly neutralizing antibodies against HIV. *Mol. Ther. J. Am. Soc. Gene Ther.* **28**, 805–819 (2020).
20. Li, L. et al. The dose of HBV genome contained plasmid has a great impact on HBV persistence in hydrodynamic injection mouse model. *Virology* **14**, 205 (2017).
21. Tankersley, C. G., Fitzgerald, R. S. & Kleeberger, S. R. Differential control of ventilation among inbred strains of mice. *Am. J. Physiol. Regul. Integr. Comp. Physiol.* **267**, R1371–R1377 (1994).
22. Kida, K., Fujino, Y. & Thurlbeck, W. M. A comparison of lung structure in male DBA and C57 black mice and their F₁ offspring. *Am. Rev. Respir. Dis.* **139**, 1238–1243 (1989).
23. Hatit, M. Z. C. et al. Species-dependent *in vivo* mRNA delivery and cellular responses to nanoparticles. *Nat. Nanotechnol.* **17**, 310–318 (2022).
24. Liu, Z. et al. Systematic comparison of 2A peptides for cloning multi-genes in a polycistronic vector. *Sci. Rep.* **7**, 2193 (2017).
25. Nelson, J. et al. Impact of mRNA chemistry and manufacturing process on innate immune activation. *Sci. Adv.* **6**, eaaz6893 (2020).
26. Altamirano-Lagos, M. J. et al. Current animal models for understanding the pathology caused by the respiratory syncytial virus. *Front. Microbiol.* **10**, 873 (2019).
27. Zost, S. J. et al. Potently neutralizing and protective human antibodies against SARS-CoV-2. *Nature* **584**, 443–449 (2020).
28. An, D. et al. Protection of K18-hACE2 mice and ferrets against SARS-CoV-2 challenge by a single-dose mucosal immunization with a parainfluenza virus 5–based COVID-19 vaccine. *Sci. Adv.* **7**, eabi5246 (2021).
29. Haque, A. K. M. A. et al. Chemically modified hCFTR mRNAs recuperate lung function in a mouse model of cystic fibrosis. *Sci. Rep.* **8**, 16776 (2018).

Publisher's note Springer Nature remains neutral with regard to jurisdictional claims in published maps and institutional affiliations.

Springer Nature or its licensor (e.g. a society or other partner) holds exclusive rights to this article under a publishing agreement with the author(s) or other rightsholder(s); author self-archiving of the accepted manuscript version of this article is solely governed by the terms of such publishing agreement and applicable law.

© The Author(s), under exclusive licence to Springer Nature Limited 2022

Methods

Polymer synthesis

Diacrylate and amine monomers were purchased from Sigma-Aldrich, Fisher and TCI America. To synthesize the hyperbranched polymers, backbone diacrylate:linear amine:trifunctional amine monomers were mostly reacted at a ratio of 1.0:0.5:0.2 with some changes for some polymers like 38 and 76 (Supplementary Table 1). The reactions were performed in anhydrous DMF at a concentration of 150 mg ml⁻¹ at 40 °C for 4 h and then 90 °C for 48 h. The resulting mixtures were allowed to cool to 30 °C and a 'capping' nucleophile (diamine, aminothiols or other functionalized amine) was added at 1.5 molar equivalent relative to the excess acrylate and the reaction was stirred for a further 24 h. The polymers were purified by dropwise precipitation into cold anhydrous diethyl ether with 0.1% glacial acetic acid, vortexed and centrifuged at 1,250×g for 2 min to pellet the polymer. The supernatant was discarded and polymer washed twice more with fresh diethyl ether and dried under a vacuum for 48 h. The polymers were stored at -20 °C. Polymer 76 is available from the corresponding author upon reasonable request.

NMR

NMR spectra were obtained on a Bruker DRX-500 or Bruker AV3 HD-700 instrument in CDCl₃ or CD₃OD. All the ¹H NMR experiments are reported in δ units, parts per million (ppm), and were measured relative to the signals for residual methanol (3.35 ppm) or chloroform (7.26 ppm).

mRNA synthesis

Plasmids containing the T7 promoter, 5' untranslated region (UTR), open reading frame and 3' UTR were used for in vitro transcription (GenScript). The sequences of the glycosylphosphatidylinositol anchor and nanoluciferase are reported elsewhere¹⁹. The *Leptotrichia buccalis* Cas13a sequence is originally obtained from Addgene (p2CT-His-MBP-Lbu_C2C2_WT, plasmid no. 83482), and the NLuc reporter sequence was placed behind a 2A cleavage site following Cas13a. The VPR sequence was originally obtained from Addgene (SP-dCas9-VPR, plasmid no. 63798) with the same 2A cleavage and NLuc sequence as above. The immunoglobulin G reporter construct was the human contraceptive antibody (HCA) sequence, originally called H6-3C4, with NLuc fused to the light chain, as discussed elsewhere^{19,30,31}.

mRNA was synthesized as previously described¹⁰. Plasmids were linearized with NotI-HF (NEB) overnight at 37 °C. Linearized templates were purified by sodium acetate (Thermo Fisher Scientific) precipitation and rehydrated with nuclease-free water. In vitro transcription was performed overnight at 37 °C using the HiScribe T7 kit (NEB) following the manufacturer's instructions (NI-methyl-pseudouridine modified). The resulting RNA was treated with DNase I (Aldevron) for 30 min to remove the template, and it was purified using lithium chloride precipitation (Thermo Fisher Scientific). The RNA was heat denatured at 65 °C for 10 min before capping with a Cap-1 structure using guanylyltransferase and 2'-O-methyltransferase (Aldevron). mRNA was then purified by lithium chloride precipitation, treated with alkaline phosphatase (NEB) and purified again. The mRNA concentration was measured using a NanoDrop instrument. The mRNA stock concentrations were 1–3 mg ml⁻¹. Purified mRNA products were analysed by gel electrophoresis to ensure purity. The crRNA N3.2 guide (5' GGACCAC-CCCAAAAUGAAGGGGACUAAAACGUAUUC AAGGCCUCUCAGUUG-CAACC 3') was purchased from Integrated DNA Technologies.

Polyplex formulation

Polyplexes were formulated as described previously¹⁰. Before delivery to animals, 100 mM of sodium acetate pH 5.0 was used to both solubilize hyperbranched PBAE and dilute mRNA before mixing. The final concentration of the mRNA was 0.5 mg ml⁻¹, and the PBAE was used at a 50× molar ratio to the mRNA. The formulations were incubated at room temperature for 10 min, and the particles were loaded into the nebulizer as described.

Dynamic light scattering measurements

Polyplexes were prepared as described for in vivo usage with a final concentration of 0.5 mg ml⁻¹ nucleic acid. Next, 10 μl of the particles was diluted into 990 μl of 100 mM sodium acetate at pH 5.0 in a sizing cuvette and analysed using a Malvern Zetasizer Nano ZS instrument. For the zeta potential measurements, 0.4 ml of the particles were diluted in 4.6 ml H₂O at pH 5.0 and loaded into a Malvern capillary for analysis.

Animal studies

Animals at the Georgia Institute of Technology and the University of Georgia were sourced and handled as described previously¹⁰.

Six- to eight-week-old female BALB/c or DBA/2 mice (Jackson Laboratories) were maintained at the Georgia Institute of Technology in individually ventilated and watered cages kept at negative pressure. BALB/c mice were used in all the experiments, unless indicated otherwise. The mice were kept in rooms on a 12 h light/dark cycle with ambient temperature between 22.8 and 23.9 °C with 30–40% relative humidity. The experiments were only performed during the light phase. Food (Lab Diet 5001) was provided to mice ad libitum. The animals were acclimatized for at least 6 days before the beginning of experiments. The animals were randomly distributed among the experimental groups. Researchers were blinded to the animal group allocation during data acquisition. The animals were euthanized by CO₂ asphyxiation. The infected animals were handled and kept under BSL-2 conditions until euthanized.

Hamster delivery optimization experiments were performed at the Georgia Institute of Technology. Four-week-old male LVG golden Syrian hamsters (Charles River Laboratories) were maintained in individually ventilated and watered cages kept at negative pressure. The hamsters were kept in rooms on a 12 h light/dark cycle with ambient temperature between 21.1 and 22.8 °C with 35–50% relative humidity. The experiments were only performed during the light phase. Food (Lab Diet 5001) was provided to hamsters ad libitum. The animals were acclimatized for at least 6 days before beginning the experiments. The animals were randomly distributed among the experimental groups. Researchers were blinded to the animal group allocation during data acquisition. The animals were euthanized by CO₂ asphyxiation.

Male, neutered and descended Fitch ferrets (Marshall BioResources) weighing about 1 kg were maintained at the Georgia Institute of Technology in wire caging with water and food provided ad libitum. The ferrets were kept in a room on a 12 h light/dark cycle with ambient temperature between 22.2 and 22.8 °C with 40–50% relative humidity. The experiments were only performed during the light phase. The ferrets were allowed -30 min of physical enrichment time three times a week. The animals were acclimatized for at least 6 days before beginning the experiments. The animals were randomly distributed among the experimental groups. Researchers were blinded to the animal group allocation during data acquisition. The animals were euthanized using approximately 2.5 ml pentobarbital-based veterinary euthanasia drug.

All the animals were cared for according to the Georgia Institute of Technology Physiological Research Laboratory policies and under ethical guidance from the university's Institutional Animal Care and Use Committee following National Institutes of Health guidelines.

Hamster infections were performed at the University of Georgia. Outbred male LVG golden Syrian hamsters, 3–4 weeks of age, were obtained from Charles River Laboratories. The hamsters were housed inside an animal BSL-3 room in a HEPA-filtered cage/rack system and provided food (Lab Diet 5053) and water ad libitum. The animals were randomly assigned to groups by the animal care staff blinded with regard to study design and treatment. The hamsters were acclimatized before use. The animals were cared for according to the University of Georgia Animal Health Research Center policies and under ethical guidance from the university's Institutional Animal Care and Use Committee following National Institutes of Health guidelines.

A normal, castrated male Holstein calf 16 weeks of age and weighing 113 kg was enrolled in the study and maintained in a paddock with access to free-choice bermudagrass hay and water and were fed a commercial calf grower ration at eight pounds daily. Before treatment, a physical exam and clinical assessment was performed and was repeated at 6, 12 and 18 h following treatment. At the conclusion of the study, the calf was euthanized via intravenous administration of Beuthanasia-D solution (390 mg ml⁻¹ pentobarbital sodium and 50 mg ml⁻¹ phenytoin sodium) at a rate of 1 ml per 4.5 kg of body weight. All the animal research activities were approved by the Mississippi State University Institutional Animal Care and Use Committee.

Rhesus macaques ($n = 3$) used in this study were housed in the BSL-2+ housing of the New Iberia Research Center and maintained in accordance with the regulations of the Guide for the Care and Use of Laboratory Animals, and the studies were reviewed and approved by the University of Louisiana at Lafayette Institutional Animal Care and Use Committee. The macaques were fed monkey chow (Purina) supplemented daily with fresh fruit or vegetables with water provided ad libitum. The animals were euthanized using 120 mg kg⁻¹ Beuthanasia delivered intravenously to animals pre-sedated with ketamine.

Nebulized mRNA polyplex delivery

Mice and hamster deliveries were performed as described previously¹⁰. The mice were loaded into a custom-built nose-only exposure system constructed of a clear polyvinyl chloride tee and animal restraints (CODA Small Mouse Holder, Kent Scientific). These were connected using a custom three-dimensionally (3D)-printed nose cone (3D Printing Tech) made of a flexible thermoplastic polyurethane material. The nebulizer (Aeroneb, Kent Scientific) was then placed on the upward-facing port of the tee. The doses were added dropwise to the nebulizer at a rate of 25 μ l per mouse per droplet. After each individual droplet was nebulized, the clear tee was inspected until the vapourized dose had cleared (approximately 15–45 s per drop). The droplets were added until the desired dose per animal was achieved. After the vapour had cleared after the last droplet, the mice were removed from the restraints.

For the delivery of mRNA to hamsters, the exposure system was modified with larger animal restraints (CODA Large Mouse Holder, Kent Scientific) and a larger 3D-printed nose cone to fit the larger restraints. To account for the increase in tidal volume in hamsters compared with mice, doses were added dropwise to the nebulizer at a rate of 62.5 μ l per hamster per droplet.

For the delivery of mRNA to ferrets, a large ferret restraint (Conduct Science) was used alongside a larger 3D-printed nose cone. Ferrets were dosed one at a time, with 100 μ l droplets added to the nebulizer at a time to account for the increase in tidal volume of the larger animals.

For the delivery of mRNA to the cow, a nose-only exposure system was created using a modified Erlenmeyer flask with a rubber gasket to seal around the snout. The end of the system was covered in several layers of gauze to collect the exhalant. An Aerogen Solo nebulizer was used with the USB power supply powered by a mobile lithium-ion battery. The complete bolus of the polyplexes was applied to the nebulizer, and the animal was allowed to breathe normally until the chamber was empty.

For the delivery of mRNA to the macaques, a paediatric nebulizer mask was used along with a U-shaped nebulizer adaptor tube (Aerogen). The macaques were only handled and dosed under sedation with an intramuscular injection of Telazol (4–8 mg kg⁻¹). The complete bolus of polyplexes was applied to the nebulizer, and the animal was allowed to breathe normally until the chamber was empty. The animals were held upright to mimic the human usage of a face-mask setup. Blood was taken via venipuncture before delivery and immediately before euthanasia.

Luminescence imaging

After euthanasia, whole lungs were collected and rinsed with phosphate-buffered saline. For mice, hamsters and ferrets, the lungs were then placed into a solution of Nano-Glo substrate (Promega)

diluted 50-fold in phosphate-buffered saline. The lungs were incubated for 5 min and then placed onto black paper and imaged with IVIS SpectrumCT (PerkinElmer). For cow and macaques, the lungs were manually sectioned using a scalpel to approximately bisect the lungs or lung lobes. Diluted Nano-Glo substrate was then dropped using a micropipette to thoroughly cover the exposed surface before imaging on the IVIS. Cow tissue was imaged on an IVIS lumina XRMS, Series III. Lung luminescence was then quantified by drawing regions of interest around the lungs using Living Image software (version 4.7.4, PerkinElmer). In each experiment, the luminescence data are presented with a single radiance range, and white lines are used to separate the groups from each other to aid visually.

SARS-CoV-2 challenge study

Hamster infections with SARS-CoV-2 were performed as described previously¹⁰. The hamsters were anaesthetized by an intraperitoneal injection of a mixture of 100 mg kg⁻¹ of ketamine per 5 mg kg⁻¹ of xylazine. After the loss of toe-pinch reflex, SARS-CoV-2 was administered to each hamster via the intranasal route in a total volume of 50 μ l. The animals were then administered a reversal agent (atipamezole, 0.15 mg kg⁻¹) and placed on a heating pad until they were able to right themselves. Body weights and clinical signs were checked and recorded daily. For sample collection, the hamsters were anaesthetized as described above and pentobarbital (100 mg kg⁻¹) was administered via intraperitoneal injection. After exsanguination and pneumothorax, the tissues were collected aseptically for analyses.

Whole lungs from individual hamsters were placed in 2 ml Dulbecco's modified Eagle medium and 1% foetal bovine serum containing antibiotics/antimycotics (D1) in C tubes and homogenized using a gentleMACS machine at the 'lung 2' setting (Miltenyi). After centrifugation for 10 min at 1,000 \times g, the supernatant was removed, and the remaining homogenates were resuspended in TRIzol for RNA extraction. Chloroform-based phase separation and RNA precipitation was then performed followed by two ethanol washes.

PCR

PCR was performed as described previously¹⁰. After total RNA quantification by NanoDrop, complementary DNA was prepared using the high-capacity complementary DNA reverse transcription kit (Applied Biosystems, Thermo Fisher Scientific). Quantitative PCR experiments were performed using the Fast Advanced Master Mix (Thermo Fisher Scientific). The anti-viral activity of Cas13a was measured ($n = 6$) by quantifying the fold change of the viral N gene using the CDC-approved N1 primer/probe set (2019-nCoV_N1) and 18S primer/probe as the endogenous control³². The experiments were performed using a QuantStudio 7 Flex thermal cycler (Applied Biosystems).

For quantification of mRNA delivery to mouse lungs, the lungs were collected 5 min after P76-mediated Cas13-2A-NLuc or aNLuc mRNA delivery (25 μ g per mouse) into 2 ml TRIzol in a Miltenyi C tube. The lungs were homogenized using the RNA_02 setting on a gentleMACS device before being aliquoted and stored at -80°C . Chloroform was added for phase separation for 15 min at 16,000 \times g. The aqueous phase containing RNA was then mixed with an equal volume of 70% ethanol and purified using an RNeasy plus kit (QIAGEN) according to the manufacturer's instructions. Complementary DNA was prepared using the RT² First Strand Kit (QIAGEN) and PCR was performed using the same Fast Advanced Master Mix (Thermo Fisher Scientific), as above, with the QuantStudio 7 Flex thermal cycler (Applied Biosystems).

Cryo-EM

Three microlitres of the sample collected before and after nebulization were placed on 300 mesh copper grids (carbon substrate with 1.2 μ m holes spaced by 1.3 μ m, Quantifoil Micro Tools). The grids were previously glow discharged (negative charge) for 15 s using a Glo-Quibe Plus glow discharge system (Quorum Tech). The samples were

blotted with filter paper for either 2.5 or 3.0 s at room temperature and 100% humidity and plunged into liquid ethane using a Vitrobot Mark IV (Thermo Fisher Scientific). The cryogenic electron microscopy (cryo-EM) grids were stored in liquid nitrogen until the cryo-EM data collection was done.

Cryo-EM images were acquired using a JEOL JEM1400 transmission electron microscope operating at 80 keV. The micrographs were collected at a nominal magnification of $\times 20,000$, on a $2,048 \times 2,048$ pixels charge-coupled device camera (UltraScan1000, Gatan), yielding a pixel size of 5.1 Å. The overview images were collected at $\times 2,000$ (52 Å per pixel). The particle diameters were determined using the measuring tool within Gatan's digital micrograph software (Gatan).

Histology and pathology scoring

Haematoxylin and eosin (H&E)-stained lung slides were examined by an American College of Veterinary Pathologists board-certified veterinary pathologist. For each animal, all the lung lobes were used for analysis and the affected microscopic fields were semiquantitatively scored as grade 0 (none), grade 1 (minimal), grade 2 (mild), grade 3 (moderate) and grade 4 (severe). Scoring was performed based on these criteria: per-cent lung affected, type-2 pneumocyte hyperplasia, alveolar septal thickening, inflammatory infiltrates and severity of bronchointerstitial pneumonia. An average and total lung score per group was calculated by combining the scores from each criterion. No significant findings were observed across any of the assayed lungs. Digital images (Fig. 4f) of H&E-stained slides were captured by the Cancer Tissue and Pathology core facility at Emory University and analysed by a board-certified pathologist. The images in Fig. 5n,o were captured by HistoWiz and analysed by a pathologist and in the same manner as above.

nCounter analysis

Tissue was collected into tubes and immediately frozen on dry ice. RNA was extracted using TRIzol as described above. RNA concentration and integrity were confirmed by a spectrophotometer and BioAnalyzer (Agilent), respectively, before being analysed on a NanoString nCounter using the mouse immunology panel according to the manufacturer's instructions. Fold changes and *p* values were calculated using the nSolver 4.0.70 software (NanoString).

Gel electrophoresis mobility retardation assay

P76 was either left unformulated or was formulated at a 50:1 mass ratio with Cas13 mRNA, crRNA or a mix of both. Unformulated RNA and polyplexes were mixed in a 1:1 ratio with RNA gel loading dye (Thermo Fisher R0641). In all the cases, 1.8 µg of Cas13a mRNA or 1.2 µg of crRNA was loaded into 1% agarose gel and ran at 80 V for 1.5 h. The gel was visualized using an Axygen Gel Documentation System-BL.

Statistical analyses

All the experiments are represented as a mean of biologically independent replicates or independent samples as indicated in the individual figure captions. Power analyses for group sizes were calculated using G*Power (version 3.1, University of Dusseldorf). Data were analysed and plotted using GraphPad Prism 9 software. Statistical analyses were performed between groups using either two-tailed *t*-tests or ordinary one-way or two-way analysis of variance (ANOVA), as specified in the individual figure captions.

Reporting summary

Further information on research design is available in the Nature Portfolio Reporting Summary linked to this article.

Data availability

Data generated or analysed during this study are provided as source data or included in the Supplementary Information. Further data are available from the corresponding authors upon request.

References

30. Tsuji, Y. et al. Human sperm carbohydrate antigens defined by an antisperm human monoclonal antibody derived from an infertile woman bearing antisperm antibodies in her serum. *J. Exp. Med.* **168**, 343–356 (1988).
31. Komori, S., Yamasaki, N., Shigeta, M., Isojima, S. & Watanabe, T. Production of heavy-chain class-switch variants of human monoclonal antibody by recombinant DNA technology. *Clin. Exp. Immunol.* **71**, 508–516 (1988).
32. Rajamäki, K. et al. Cholesterol crystals activate the NLRP3 inflammasome in human macrophages: a novel link between cholesterol metabolism and inflammation. *PLoS ONE* **5**, e11765 (2010).

Acknowledgements

We would like to acknowledge the substantial help of the animal support staff at the four institutions: Georgia Institute of Technology Physiological Research Laboratory (PRL); Mississippi State University; The University of Georgia Animal Health Research Center (AHRC); and the University of Louisiana at Lafayette, New Iberia Research Center (NIRC). IVIS imaging at the Mississippi State University was supported through USDA-ARS Biophotonics Initiative #58-6402-3-018. We would like to acknowledge the pathology core facilities at the Yerkes National Primate Research Center and UGA for histology and tissue preparation work. We would also like to acknowledge V. Parihar of the Cancer Tissue and Pathology and Lya Griffiths of the Emory Integrated Genomic Core (EIGC) for their help on slide scanning and nCounter analysis, respectively. The cryo-EM was supported by the Robert P. Apkarian Integrated Electron Microscopy Core. We would also like to acknowledge the University of Louisiana Lafayette-NIRC Clinical Pathology Laboratory for their work with preparing and analysing the macaque bloodwork as well as C. Carter for performing the Magpix cytokine analysis. We would also like to acknowledge J. E. Crowe, Vanderbilt University Vaccine Center, for supplying COV2-2381 for the SARS-CoV-2 experiments. Computational work used the Hive cluster, which is supported by the National Science Foundation under grant no. 1828187 and is managed by the Partnership for an Advanced Computing Environment (PACE) at the Georgia Institute of Technology. Figures 1b,c, 4b and 6d were created in part using BioRender.com. This study was supported by the Defense Advanced Research Projects Agency, grant no. HR00111920008.

Author contributions

P.J.S. conceived the overall project. L.R., N.C.B. and M.G.F. designed the polymer synthesis approach. L.R. and N.C.B. synthesized the polymers. L.R., D.V., H.E.P., C.Z., R.K.N., L.O., J.Y.J. and L.C.S.C. performed the mouse, hamster and ferret studies at Georgia Tech. J.Y.J. and Y.J. performed the in vitro studies. H.E.P. synthesized all the mRNA used in the study. S.G. and A.K.O. analysed the histology samples. L.R., D.V., S.C., M.T. and A.R.W. performed the bovine study. L.R., D.V., M.A. and F.V. performed the macaque study. D.V., C.Z., J.M., N.O.-B., E.R.L. and R.J.H. performed the hamster SARS-CoV-2 challenge. L.R., D.V. and J.B. conducted the dynamic light scattering measurements. L.R., D.V. and R.G.-F. performed the cryo-EM studies. D.V., C.Z. and J.B. conducted the FISH and microscopy experiments and analysis. K.M.K. and J.C.G. performed the computational molecular dynamic modelling. L.R., D.V., C.Z. and P.J.S. designed the experiments, interpreted the data and wrote the manuscript. All the authors reviewed and edited the paper.

Competing interests

L.R., D.V., N.C.B., M.G.F. and P.J.S. have a provisional patent filing (Application No. 63/287,691) related to this work. D.V., C.Z. and P.J.S. are cofounders of Tether Therapeutics. This study could affect their

personal financial statuses. The terms of these arrangements have been reviewed and approved by Emory University in accordance with its conflict-of-interest policies. All other authors declare no competing interests.

Additional information

Supplementary information The online version contains supplementary material available at <https://doi.org/10.1038/s41563-022-01404-0>.

Correspondence and requests for materials should be addressed to Philip J. Santangelo.

Peer review information *Nature Materials* thanks Liangfang Zhang and the other, anonymous, reviewer(s) for their contribution to the peer review of this work.

Reprints and permissions information is available at www.nature.com/reprints.

Reporting Summary

Nature Portfolio wishes to improve the reproducibility of the work that we publish. This form provides structure for consistency and transparency in reporting. For further information on Nature Portfolio policies, see our [Editorial Policies](#) and the [Editorial Policy Checklist](#).

Statistics

For all statistical analyses, confirm that the following items are present in the figure legend, table legend, main text, or Methods section.

n/a Confirmed

- The exact sample size (n) for each experimental group/condition, given as a discrete number and unit of measurement
- A statement on whether measurements were taken from distinct samples or whether the same sample was measured repeatedly
- The statistical test(s) used AND whether they are one- or two-sided
Only common tests should be described solely by name; describe more complex techniques in the Methods section.
- A description of all covariates tested
- A description of any assumptions or corrections, such as tests of normality and adjustment for multiple comparisons
- A full description of the statistical parameters including central tendency (e.g. means) or other basic estimates (e.g. regression coefficient) AND variation (e.g. standard deviation) or associated estimates of uncertainty (e.g. confidence intervals)
- For null hypothesis testing, the test statistic (e.g. F , t , r) with confidence intervals, effect sizes, degrees of freedom and P value noted
Give P values as exact values whenever suitable.
- For Bayesian analysis, information on the choice of priors and Markov chain Monte Carlo settings
- For hierarchical and complex designs, identification of the appropriate level for tests and full reporting of outcomes
- Estimates of effect sizes (e.g. Cohen's d , Pearson's r), indicating how they were calculated

Our web collection on [statistics for biologists](#) contains articles on many of the points above.

Software and code

Policy information about [availability of computer code](#)

Data collection No software was used for data collection.

Data analysis Data plotting and statistical analysis was performed in Graphpad Prism 9. Nanostring analysis fold changes and p-values were calculated using the nSolver 4.0.70 software. Slide scans of RNAscope images were analyzed and presented using QuPath 0.3.0. Percent positive analyses were completed using Bitplane Imaris 9.7.2. Particle diameters from cryoEM images were determined using the measuring tool within Gatan's Digital Micrograph 2.31.734.0 software. High resolution confocal images were analyzed and presented using Volocity version 6.3.1. Luminescence from all organs was measured and analyzed using Perkin Elmer Living Image 4.7.4. Flow cytometry data was analyzed using Flowjo version 10.7.0. Serum cytokine concentrations were calculated using xPONENT 4.2 software. The molecular dynamics simulations were completed using: Visual Molecular Dynamics (VMD 1.9.4a38), the Molefacture plugin 2.0 of VMD, NAMD, NAMD2, CGenFF, and CHARMM36.

For manuscripts utilizing custom algorithms or software that are central to the research but not yet described in published literature, software must be made available to editors and reviewers. We strongly encourage code deposition in a community repository (e.g. GitHub). See the Nature Portfolio [guidelines for submitting code & software](#) for further information.

Data

Policy information about [availability of data](#)

All manuscripts must include a [data availability statement](#). This statement should provide the following information, where applicable:

- Accession codes, unique identifiers, or web links for publicly available datasets
- A description of any restrictions on data availability
- For clinical datasets or third party data, please ensure that the statement adheres to our [policy](#)

Data generated or analysed during this study are provided as Source Data or included in the Supplementary Information. Further data are available from the corresponding authors upon request.

Field-specific reporting

Please select the one below that is the best fit for your research. If you are not sure, read the appropriate sections before making your selection.

- Life sciences Behavioural & social sciences Ecological, evolutionary & environmental sciences

For a reference copy of the document with all sections, see [nature.com/documents/nr-reporting-summary-flat.pdf](https://www.nature.com/documents/nr-reporting-summary-flat.pdf)

Life sciences study design

All studies must disclose on these points even when the disclosure is negative.

Sample size	Power analyses for group sizes were calculated using G*Power (version 3.1, University of Dusseldorf).
Data exclusions	No data was excluded from the analysis.
Replication	Molecular dynamic simulations were completed 3 times for each system. Animal experiments were completed once with n animals per group, as described in the caption of each figure.
Randomization	Animals were allocated randomly into groups in all experiments.
Blinding	The Emory and Georgia Tech researchers were blinded to the hamster weight data generated at the University of Georgia and to all of the macaque data generated at the University of Louisiana Lafayette New Iberia Research Center. Additionally, the Emory EIGC core facility and Antech were blinded to the group choices during data acquisition. Pathologist scoring was performed blinded after initial inspection for parameter selection.

Reporting for specific materials, systems and methods

We require information from authors about some types of materials, experimental systems and methods used in many studies. Here, indicate whether each material, system or method listed is relevant to your study. If you are not sure if a list item applies to your research, read the appropriate section before selecting a response.

Materials & experimental systems

n/a	Involved in the study
<input checked="" type="checkbox"/>	<input type="checkbox"/> Antibodies
<input type="checkbox"/>	<input checked="" type="checkbox"/> Eukaryotic cell lines
<input checked="" type="checkbox"/>	<input type="checkbox"/> Palaeontology and archaeology
<input type="checkbox"/>	<input checked="" type="checkbox"/> Animals and other organisms
<input checked="" type="checkbox"/>	<input type="checkbox"/> Human research participants
<input checked="" type="checkbox"/>	<input type="checkbox"/> Clinical data
<input checked="" type="checkbox"/>	<input type="checkbox"/> Dual use research of concern

Methods

n/a	Involved in the study
<input checked="" type="checkbox"/>	<input type="checkbox"/> ChIP-seq
<input checked="" type="checkbox"/>	<input type="checkbox"/> Flow cytometry
<input checked="" type="checkbox"/>	<input type="checkbox"/> MRI-based neuroimaging

Eukaryotic cell lines

Policy information about [cell lines](#)

Cell line source(s)	Expi293F (A14527) from Thermo Fisher and A549 (CCL-185) from ATCC.
Authentication	The cell lines used in this study were authenticated by the supplier.
Mycoplasma contamination	Cells were routinely tested for mycoplasma contamination.

Animals and other organisms

Policy information about [studies involving animals](#); [ARRIVE guidelines](#) recommended for reporting animal research

Laboratory animals

BALB/c and DBA/2 mice (females, 6-8 weeks old from Jackson Laboratories); Golden Syrian Hamsters (males, 4 weeks old from Charles River Laboratories); Fitch ferrets (neutered and descended males, 3 months old from Marshall BioResources); Holstein calf (castrated male, 16 weeks old); Rhesus macaque (females, 11 and 19 years old)

Wild animals

The study did not involve wild animals.

Field-collected samples

The study did not involve field-collected samples

Ethics oversight

At the Georgia Institute of Technology, all animals were cared for according to the Georgia Institute of Technology Physiological Research Laboratory policies and under ethical guidance from the university's Institutional Animal Care and Use Committee (IACUC) following National Institutes of Health (NIH) guidelines. At the University of Georgia, animals were cared for according to the University of Georgia Animal Health Research Center policies and under ethical guidance from the university's IACUC following NIH guidelines. At the Mississippi State University, animal research activities were approved by the Mississippi State University IACUC. At the New Iberia Research Center at the University of Louisiana at Lafayette, animals were maintained in accordance with the regulations of the Guide for the Care and Use of Laboratory Animal, and the studies were reviewed and approved by the University of Louisiana at Lafayette IACUC.

Note that full information on the approval of the study protocol must also be provided in the manuscript.